



# Coherent emission from surface Josephson plasmons in striped cuprates

D. Nicoletti<sup>a,1</sup>, M. Buzzi<sup>a</sup>, M. Fechner<sup>a</sup>, P. E. Dolgirev<sup>b</sup>, M. H. Michael<sup>a,b</sup>, J. B. Curtis<sup>b,c</sup>, E. Demler<sup>d</sup>, G. D. Gu<sup>e</sup>, and A. Cavalleri<sup>a,f</sup>

Edited by Angel Rubio, Max-Planck-Institut für Struktur und Dynamik der Materie, Hamburg, Germany; received July 8, 2022; accepted August 5, 2022

The interplay between charge order and superconductivity remains one of the central themes of research in quantum materials. In the case of cuprates, the coupling between striped charge fluctuations and local electromagnetic fields is especially important, as it affects transport properties, coherence, and dimensionality of superconducting correlations. Here, we study the emission of coherent terahertz radiation in single-layer cuprates of the  $\text{La}_{2-x}\text{Ba}_x\text{CuO}_4$  family, for which this effect is expected to be forbidden by symmetry. We find that emission vanishes for compounds in which the stripes are quasi-static but is activated when  $c$ -axis inversion symmetry is broken by incommensurate or fluctuating charge stripes, such as in  $\text{La}_{1.905}\text{Ba}_{0.095}\text{CuO}_4$  and in  $\text{La}_{1.845}\text{Ba}_{0.155}\text{CuO}_4$ . In this case, terahertz radiation is emitted by surface Josephson plasmons, which are generally dark modes, but couple to free space electromagnetic radiation because of the stripe modulation.

terahertz emission | cuprates | superconductivity | stripes | surface Josephson plasmons

Nonlinear terahertz (THz) spectroscopy has recently emerged as a new tool to study the microscopic properties of quantum materials, being susceptible to the symmetry of low-energy degrees of freedom and complementing already-existing nonlinear optical probes (1). For example, THz third-harmonic generation was shown to be a sensitive probe of superfluid stripes, which do not couple to light at linear order but participate in higher-order responses (2, 3). As such, the study of THz nonlinear optics in presence of frustrated couplings provides new opportunities to explore the symmetry of quantum materials. Here, we focus on THz emission from high- $T_C$  cuprates and demonstrate how this method is highly sensitive to the spatial arrangement of the superconducting state and its interaction with *charge-stripe order*.

The emission of THz radiation from materials illuminated with femtosecond optical pulses (4–7) is generally enabled by two classes of mechanisms. The first mechanism, active in transparent noncentrosymmetric materials such as ZnTe or LiNbO<sub>3</sub>, is based on optical rectification, where the second-order nonlinear optical susceptibility causes a time-dependent electrical polarization (8). The second mechanism relies on the excitation of time-dependent charge currents and is well documented for biased high-mobility semiconductors (8). A number of additional reports of coherent THz radiation have been made for complex quantum materials, typically related to the perturbation of electronic and magnetic interactions. THz emission in colossal magnetoresistance manganites (7, 9, 10), magnetic and multiferroic compounds (11–20), are some of the best-known examples.

In the case of high- $T_C$  superconductors, coherent THz emission has been reported only for situations in which time-dependent supercurrents,  $\vec{J}_s(t)$ , are set in (8). These situations range from near-single-cycle THz pulses in biased antennae fabricated from  $\text{YBa}_2\text{Cu}_3\text{O}_{7-\delta}$  or  $\text{Bi}_2\text{Sr}_2\text{CaCu}_2\text{O}_{8+\delta}$  films (5, 21, 22), to multicycle narrowband emissions governed by the Josephson effect in the case of applied out-of-plane magnetic fields (23). It has also been shown that the use of Josephson junction stacks in mesatype resonant structures allows orders of magnitude increase in THz emission efficiency, also providing narrow bandwidths and tuneable frequency (24–26).

Here, we report anomalous THz emission in high- $T_C$  cuprates, observed for photoexcitation with femtosecond near-infrared pulses, in absence of external magnetic fields and current biases. The effect is detected only when superconductivity coexists with charge-stripe order in the Cu-O planes (27–30) and when these stripes are either incommensurate with the lattice or fluctuating.

We studied cuprates belonging to the “214” family, with one Cu-O layer per unit cell. As a prototypical “homogeneous” cuprate, we considered optimally doped  $\text{La}_{2-x}\text{Sr}_x\text{CuO}_4$  (LSCO), with a critical temperature of 38 K (phase diagram in Fig. 1A). Although in the LSCO family fluctuating striped charge and spin orders have been reported in the underdoped region of the phase diagram (31), there is no evidence for stripes at optimal 0.16 doping (32). This sample was compared with the response of

## Significance

We observe anomalous terahertz emission in photo-excited high- $T_C$  cuprates with coexisting superconductivity and charge-stripe order, in absence of any external magnetic field or current bias. Because this phenomenon should be forbidden by symmetry, our observation indicates a symmetry breaking in the stripe phase. The emission spectrum reveals the excitation of surface Josephson plasmons, which are generally dark modes but become coupled to the electromagnetic continuum in these materials by the presence of stripes. The study of coherent anomalous terahertz emission emerges as a sensitive tool to probe the symmetry of superconductors in the presence of frustrated couplings, which is a key topic in the physics of these materials.

Author affiliations: <sup>a</sup>Max Planck Institute for the Structure and Dynamics of Matter, 22761 Hamburg, Germany; <sup>b</sup>Department of Physics, Harvard University, Cambridge, MA 02138; <sup>c</sup>John A. Paulson School of Engineering and Applied Sciences, Harvard University, Cambridge, MA 02138; <sup>d</sup>Institute for Theoretical Physics, ETH Zurich, 8093 Zurich, Switzerland; <sup>e</sup>Condensed Matter Physics and Materials Science Department, Brookhaven National Laboratory, Upton, NY 11973; and <sup>f</sup>Department of Physics, Clarendon Laboratory, University of Oxford, Oxford OX1 3PU, United Kingdom

Author contributions: D.N., M.B., E.D., and A.C. designed research; D.N., M.B., M.F., P.E.D., M.H.M., J.B.C., E.D., G.D.G., and A.C. performed research; D.N. and M.B. analyzed data; and D.N., M.B., and A.C. wrote the paper.

The authors declare no competing interest.

This article is a PNAS Direct Submission.

Copyright © 2022 the Author(s). Published by PNAS. This open access article is distributed under Creative Commons Attribution License 4.0 (CC BY).

<sup>1</sup>To whom correspondence may be addressed. Email: daniele.nicoletti@mpsd.mpg.de.

This article contains supporting information online at <http://www.pnas.org/lookup/suppl/doi:10.1073/pnas.2211670119/-DCSupplemental>.

Published September 20, 2022.

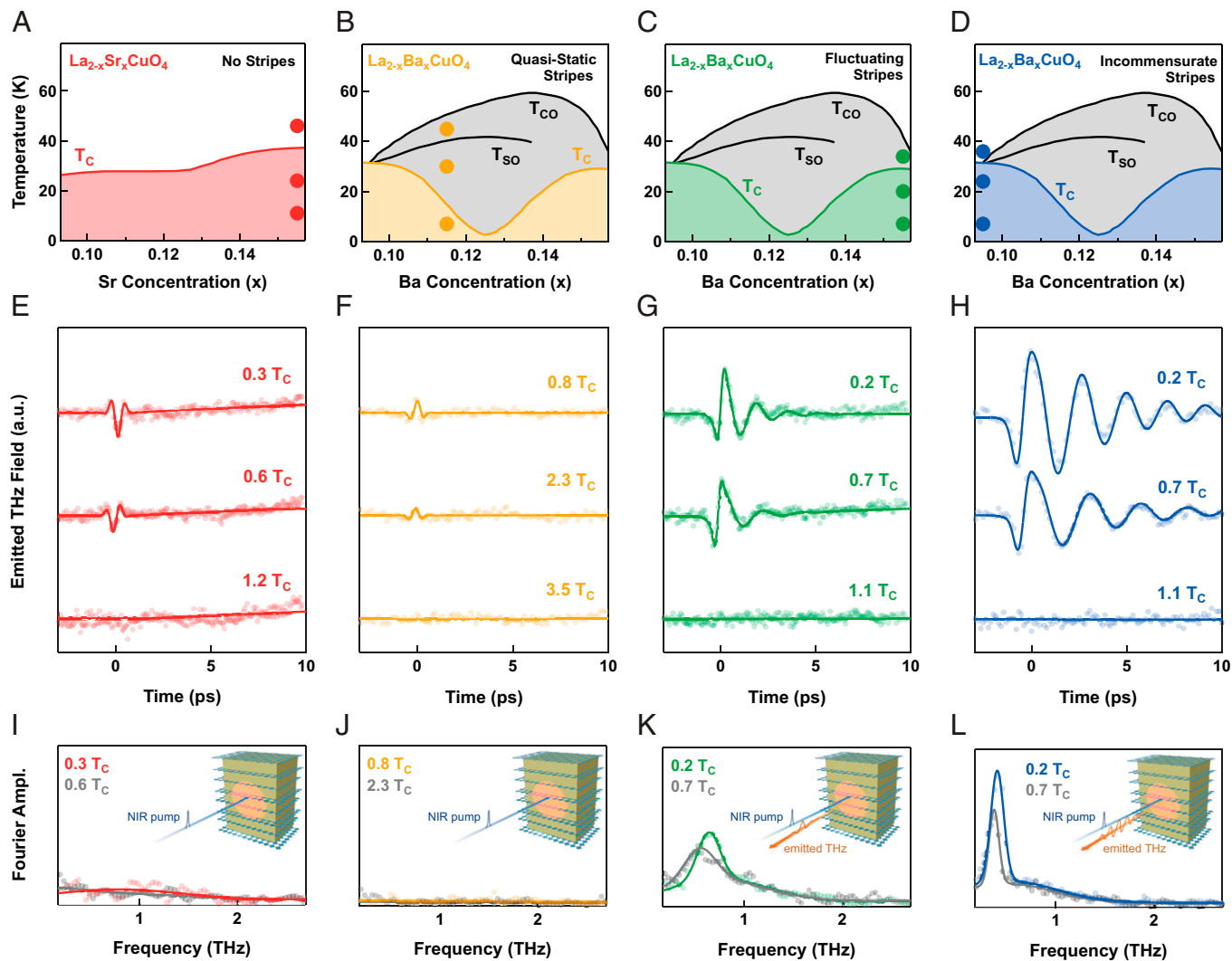


**Fig. 1.** (A–D) Temperature-doping phase diagrams of the four compounds investigated in the present study.  $T_{CO}$ ,  $T_{SO}$ , and  $T_C$  stand for the charge ordering, the spin ordering, and the superconducting critical temperature, respectively. (E–H) Time-dependent THz emission traces taken for a pump fluence of  $2.5 \text{ mJ/cm}^2$  at the temperatures indicated by full circles in (A–D). Solid lines represent multicomponent fits to the data (SI Appendix). The vertical scales in the three panels are mutually calibrated. (I–L) Fourier transforms (circles) of selected time-domain traces in (E–H). Solid lines are multi-Gaussian fits. *Insets:* Experimental geometry. Near-infrared (NIR) pump pulses are shone at normal incidence onto an *ac*-oriented sample surface, with polarization parallel to the *c* axis. As a result of photoexcitation, *c*-polarized THz radiation is emitted. Ampl., amplitude.

$\text{La}_{2-x}\text{Ba}_x\text{CuO}_4$  (LBCO), for which superconductivity coexists with charge stripes (27). We focused on three LBCO compounds:  $\text{La}_{1.885}\text{Ba}_{0.115}\text{CuO}_4$  (LBCO 11.5%,  $T_C = 13 \text{ K}$ ), where the superconducting transition is highly depleted by a robust stripe phase below the charge ordering temperature  $T_{CO} = 53 \text{ K}$ ,  $\text{La}_{1.845}\text{Ba}_{0.155}\text{CuO}_4$  (LBCO 15.5%,  $T_C = 30 \text{ K}$ ,  $T_{CO} = 40 \text{ K}$ ), placed at the nominal optimal doping and characterized by weak, highly fluctuating stripes (27), and  $\text{La}_{1.905}\text{Ba}_{0.095}\text{CuO}_4$  (LBCO 9.5%,  $T_C = T_{CO} = 33 \text{ K}$ ), for which the stripes have an intermediate intensity and correlation length compared with the other two compounds (27), but in contrast to them are here highly incommensurate (33, 34). The location of the three samples in the LBCO phase diagram is shown in Fig. 1 B–D.

We note that LBCO is the same cuprate in which signatures of optically enhanced superconductivity have been measured (35–38) and attributed to the ultrafast perturbation of the stripe order (39, 40). In addition, a number of nonlinear optical effects, such as THz parametric amplification (41) and third-harmonic generation (2), related to the resonant driving of Josephson plasma waves, have also been measured.

The main result of our experiment is summarized in Fig. 1 E–L, where the measured THz emission traces are reported for the four investigated compounds for selected temperatures, at a constant pump fluence of  $2.5 \text{ mJ/cm}^2$ . The experimental geometry is shown in the insets of the lower panels. We used the output of an amplified Ti:Sa laser as pump pulses, with a duration of 100 fs and photon energy of 1.55 eV (800 nm wavelength). These were focused at normal incidence onto an *ac*-oriented sample surface on an  $\sim 500 \mu\text{m}$  spot. The emitted THz pulses were collimated with a parabolic mirror and refocused on a 1-mm-thick ZnTe crystal to perform electro-optic sampling directly yielding THz electric field traces in time domain.

In optimally doped LSCO (Fig. 1 E), the THz emission signal was measurable only in the superconducting state below  $T_C$  and displayed a very small amplitude, just above the noise level. This effect consisted of a single-cycle trace, with a flat and featureless spectrum (Fig. 1 I). A similar response was also found in LBCO 11.5% (Fig. 1 F and J), where charge stripes are robust, quasi-static, and quasi-commensurate. Here, a barely detectable emission signal was also found for  $T > T_C$ .

On the other hand, in LBCO 15.5% [weak, highly fluctuating, but quasi-commensurate stripes (33, 34) (Fig. 1 G and K),

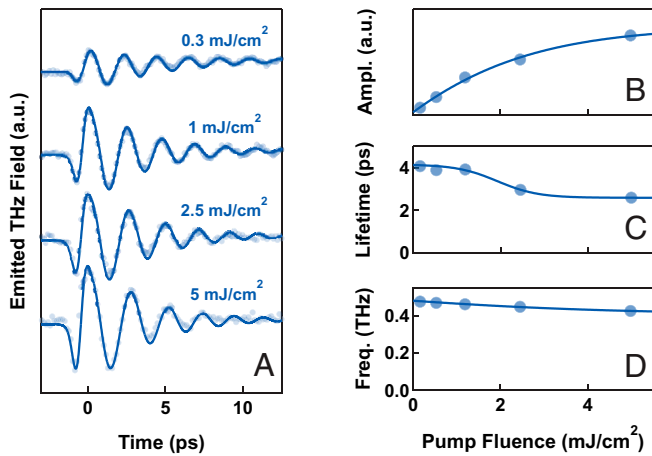


**Fig. 2.** Pump fluence-dependent THz emission in  $\text{La}_{1.905}\text{Ba}_{0.095}\text{CuO}_4$  at  $T = 7$  K. (A) Experimental traces taken for different pump fluences (full circles). Solid lines are multicomponents fits to the data, which include a quasi-monochromatic, long-lived oscillation and a “single-cycle” component around time 0 (*SI Appendix*). (B–D) Fluence-dependent parameters of the quasi-monochromatic oscillation extracted from the fits in (A). Ampl., amplitude; Freq., frequency.

the THz emission in the superconducting state acquired an appreciable amplitude, with oscillations at a frequency of  $\sim 600$  GHz (depending on temperature).

In the compound with incommensurate, relatively strong stripes, i.e., LBCO 9.5%, the THz emission amplitude was even higher than LBCO 15.5% and greater by a factor of  $\sim 5$ – $10$  compared with LSCO and LBCO 11.5%. Coherent multicycle oscillations were observed (Fig. 1*H*), corresponding to a narrow spectral peak (Fig. 1*L*). The frequency of these oscillations shifted to the red with increasing temperature, while also reducing in amplitude and disappearing at  $T_C$ .

The rest of the analysis in this paper is focused on LBCO 9.5%, which yielded the largest signal and highest coherence. We verified that the emission was entirely polarized along the out-of-plane crystallographic axis and could be induced only for a pump polarization aligned along the same direction (*SI Appendix*).

Fig. 2*A* displays the pump fluence dependence measured at a constant temperature of 7 K. These experimental traces were modeled using fits in time domain (solid lines), for which we report the single components in the *SI Appendix*. These include

a “single-cycle” pulse at early times, which was absent at the lowest fluences and grew quadratically with irradiation, and a quasi-monochromatic, long-lived oscillation, which grew linearly up to about  $1 \text{ mJ/cm}^2$  and tended to saturate for higher excitation fluence (Fig. 2*B*). This linear trend of the main oscillation is compatible with the impulsive excitation of a coherent mode. In the fluence-dependent behavior of lifetime and oscillation frequency (Fig. 2*C* and *D*), we identify a linear excitation regime where these quantities are weakly dependent on fluence and seem to stabilize at constant values of  $\sim 4$  ps and  $\sim 0.45$  THz, respectively. In this weak excitation regime, the driven mode parameters are well determined.

In Fig. 3, we report the temperature dependence of this effect. We show a comparison between the oscillation frequency in the THz emission signal in LBCO 9.5%, and the bulk Josephson plasma resonance measured at equilibrium with time-resolved THz spectroscopy in the same sample. In the inset of Fig. 3*A*, we show the experimental geometry in which we illuminated the sample with weak broadband THz pulses (generated in a  $200\text{-}\mu\text{m}$ -thick GaP), polarized along the out-of-plane direction, that were then detected in another  $200\text{-}\mu\text{m}$ -thick GaP crystal via electro-optic sampling after being reflected from the sample surface.

Fig. 3*A* displays examples of reflectivity ratios at two temperatures below  $T_C$ , normalized by the same quantity measured in the normal state. These curves evidence a Josephson plasma resonance, the exact frequency of which was determined by fitting the experimental data with a Josephson plasma model (solid lines) (35, 38). The key result of this analysis is displayed in Fig. 3*B*, in which we show a comparison of the temperature dependence of the Josephson plasma frequency at equilibrium (gray) with the frequency of the emitted oscillations for two pump fluences. Notably, the emitted mode frequency hardens with decreasing fluence and approaches the equilibrium plasma frequency measured at the corresponding base temperature.

In interpreting our results, we first note that in a centrosymmetric cuprate, impulsive excitation of Josephson plasmons is forbidden by symmetry. Josephson plasma modes are in fact symmetry-odd (infrared-active), while impulsive photoexcitation couples only to totally symmetric modes (42). As discussed in a related theory work (43), a prerequisite for the excitation of these modes is that charge order breaks inversion symmetry. However, this does not happen for commensurate quasi-static stripes as

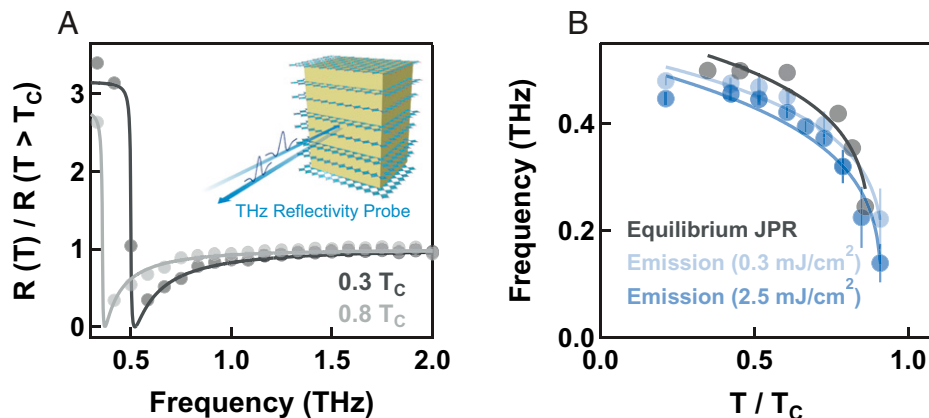


**Fig. 3.** Comparison with the equilibrium Josephson plasma resonance (JPR) in  $\text{La}_{1.905}\text{Ba}_{0.095}\text{CuO}_4$ . (A, *Inset*) Experimental geometry for the equilibrium THz time-domain characterization. A weak broadband THz pulse was shone at normal incidence onto the sample surface with polarization along the  $c$  direction. The electric field profile of the same THz pulse was then detected after reflection. (A) Reflectivity taken at two different temperatures in the superconducting state, normalized by the same quantity measured at  $T = 35 \text{ K} > T_C$  (full circles). The solid lines are fits to the data performed with a JPR model. (B) Temperature dependence of the equilibrium Josephson plasma frequency (gray circles), as determined from the fits in (A). The oscillation frequencies in the THz emission signal measured in the same sample are also reported for two different excitation fluences (legend). Error bars indicate uncertainties extracted from fits such as those in Fig. 2 (see also *SI Appendix*). Solid lines are guides to the eye.

those expected for dopings  $x \geq 1/8$  (33, 34), which exhibit a twofold screw axis along the out-of-plane direction (see Fig. 4A) (44). A symmetry breaking is expected instead for incommensurate or highly fluctuating stripes, as in the case of LBCO 9.5% and LBCO 15.5%. Here, the charge order correlation length along the out-of-plane direction is of the order of one unit cell (27), resulting in a loss of the phase relation between stripes in next-nearest-neighbor planes (Fig. 4B).

Once inversion symmetry is broken, electromagnetic emission at a frequency  $\omega \ll \omega_{pump}$  can result from rectification of the optical pulse. We associate the optically rectified drive for plasma oscillations with the excitation of a *shift current* (43, 44) at the sample surface. This is expected to interact with modes at  $\omega \simeq \omega_{JPR}$ , of which one finds at least two: 1) a *bulk Josephson plasma polariton*, sustained by tunneling supercurrents oriented in the  $z$  (out-of-plane) direction and propagating along the  $x$  (in-plane) direction; and 2) a *surface Josephson plasmon*, also sustained by plasma oscillations in the  $z$  direction, but localized at the surface of the material and propagating along  $z$ . The dispersion relations for these two modes are shown in Fig. 4C and D, respectively (45).

Radiation from bulk plasma polaritons (Fig. 4C), excited over a depth between  $\sim 200$  nm (skin depth of the pump) and  $\sim 1 \mu\text{m}$  (46), would be expected to be broad in frequency and overdamped. This is because excitation by the near-infrared pump covers a wide range of in-plane momenta,  $q_x$ , which in the first instance, is limited only by the envelope bandwidth of the pump pulse (gray shading in Fig. 4C). The spectrum of Josephson plasmons would, in this case, also be independent of the details of the stripe order and of its correlation lengths, as is instead observed. Moreover, one would expect radiation at frequencies  $\omega \gtrsim \omega_{JPR}$ , in contrast to the experimental observation of a slightly redshifted emission with respect to the plasma frequency (Fig. 3B).

Coherent narrowband emission by surface Josephson plasmons is instead more likely. Although the dispersion of these modes lies below the light cone and, hence, they are not expected to radiate into vacuum (Fig. 4D), we argue here that Bragg scattering off the stripe order induces a backfolding, defined by the stripe wave vector, into a reduced Brillouin zone (dashed horizontal line in Fig. 4D). For this reason, these surface modes can radiate, much like a situation in which a fabricated corrugation would be used to achieve the coupling (47–50).

In the right panel of Fig. 4D, we report the emission spectrum calculated for a striped superconductor through the excitation of surface Josephson plasmons. As extensively discussed in our related theory work (43, 44), in the presence of stripes, the pump pulse is expected to give origin to an *Umklapp* shift current,  $J_U \cos(Q_{stripes} z)$ , that is modulated in space by the stripe wave vector,  $Q_{stripes}$ . This naturally drives high-momenta surface plasmons, which can radiate out due to the aforementioned backfolding mechanism.

In summary, we have reported the observation of coherent THz emission just below the Josephson plasma frequency in cuprates for which the superconducting state coexists with stripes. We assigned this effect to the excitation of surface Josephson plasmons, which become Raman active due to the breaking of inversion symmetry induced by the stripes and can radiate out thanks to the backfolding of their dispersion curve onto the light cone. Based on these findings, the characterization of coherent THz emission emerges as a sensitive method to unveil broken symmetry states, which may not be detectable with other conventional techniques. Moreover, the absence of

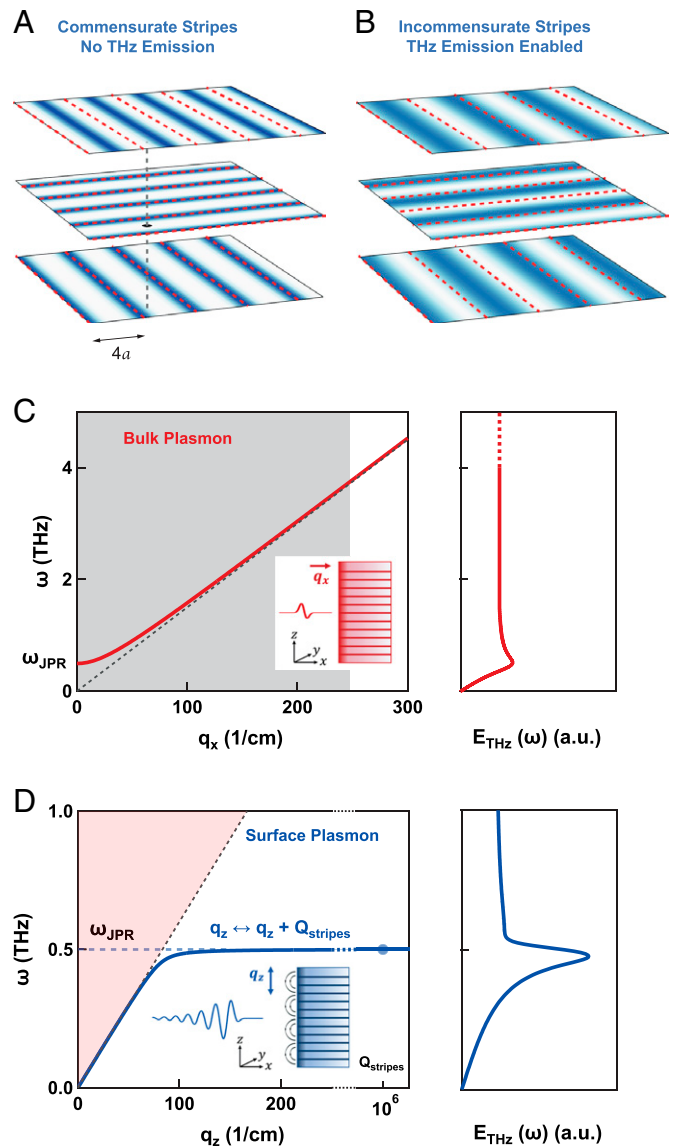


**Fig. 4.** (A) Charge density pattern (gradual scale of blue) in three neighboring planes of a cuprate with commensurate stripes (red dashed lines are spaced by  $4a$ , where  $a$  is the lattice constant). Stripes in next-nearest layers are off-phased by  $\pi$  (30). Here, inversion symmetry is preserved (black dot and vertical dashed line are an inversion center and a screw axis, respectively). (B) Once commensurability is lost, stripes are fluctuating, or there is no phase relation between next-nearest layers, inversion symmetry can be broken, and THz emission is enabled (43). (C, Left) In-plane dispersion of bulk Josephson plasma polaritons (red line). Emission from these modes (Right) is expected to be very broad, as it encompasses a wide range of in-plane momenta,  $q_x$  (gray shading) (43). (D, Left) Out-of-plane dispersion of surface Josephson plasmons (solid blue line). These modes are localized at the surface and propagate along  $z$  (out-of-plane direction). As their dispersion lies below the light cone (red shading), they are not expected to radiate into vacuum. However, Bragg scattering off the stripe order induces a backfolding, defined by the stripe wave vector,  $Q_{stripes}$ , into a reduced Brillouin zone (dashed horizontal line). Hence, these surface modes are redirected into the light cone and can radiate out at frequencies just below  $\omega_{JPR}$  ( $q = 0$ ). (Right) Calculated emission spectrum from surface Josephson plasmons in a striped superconductor (43). JPR, Josephson plasma resonance.

THz emission in LBCO 11.5%, where the stripes are more robust and quasi-static, may suggest a qualitative difference in the nature of charge and spin order between compounds that are in the vicinity of the commensurate 1/8 doping and those that are far from it.

**Data, Materials, and Software Availability.** All study data are included in the article and/or *SI Appendix*.

**ACKNOWLEDGMENTS.** The research leading to these results received funding from the European Research Council under the European Union's Seventh Framework Programme (FP7/2007-2013)/ERC Grant Agreement No. 319286 (QMAC). We acknowledge support from the Deutsche Forschungsgemeinschaft (German Research Foundation) via the excellence cluster "CUI: Advanced Imaging of Matter" (EXC 2056, project ID 390715994) and the priority program SFB925 (project ID 170620586). E.D. acknowledges support from AFOSR-MURI: Photonic Quantum Matter award FA95501610323, DARPA DRINQS, the ARO

grant "Control of Many-Body States Using Strong Coherent Light-Matter Coupling in Terahertz Cavities." J.B.C. is supported by the Quantum Science Center, a National Quantum Information Science Research Center of the US Department of Energy, and by the Harvard Quantum Initiative. J.B.C. also acknowledges hospitality from the Max Planck Institute for Structure and Dynamics of Matter (Hamburg), and ETH Zürich Institute for Theoretical Physics. Work at Brookhaven is supported by the Office of Basic Energy Sciences, Division of Materials Sciences and Engineering, US Department of Energy, under Contract No. DE-SC0012704.

1. L. Zhao *et al.*, A global inversion-symmetry-broken phase inside the pseudogap region of  $\text{YBa}_2\text{Cu}_3\text{O}_y$ . *Nat. Phys.* **13**, 250–254 (2017).
2. S. Rajasekaran *et al.*, Probing optically silent superfluid stripes in cuprates. *Science* **359**, 575–579 (2018).
3. D. Fu *et al.*, Terahertz phase slips in striped  $\text{La}_{2-x}\text{Ba}_x\text{CuO}_4$ . *Phys. Rev. B* **105**, L020502 (2022).
4. D. H. Auston, K. P. Cheung, P. R. Smith, Picosecond photoconducting Hertzian dipoles. *Appl. Phys. Lett.* **45**, 284 (1984).
5. M. Hangyo *et al.*, Terahertz radiation from superconducting  $\text{YBa}_2\text{Cu}_3\text{O}_{7-\delta}$  thin films excited by femtosecond optical pulses. *Appl. Phys. Lett.* **69**, 2122 (1996).
6. T. Kiwa, I. Kawashima, S. Nashima, M. Hangyo, M. Tonouchi, Optical response in amorphous GaAs thin films prepared by pulsed laser deposition. *Jpn. J. Appl. Phys.* **39**, 6304 (2000).
7. N. Kida, M. Tonouchi, Terahertz radiation from magnetoresistive  $\text{Pr}_{0.7}\text{Ca}_{0.3}\text{MnO}_3$  thin films. *Appl. Phys. Lett.* **78**, 4115 (2001).
8. D. S. Rana, M. Tonouchi, Terahertz emission functionality of high-temperature superconductors and similar complex systems. *Adv. Opt. Mater.* **8**, 1900892 (2020).
9. N. Kida, K. Takahashi, M. Tonouchi, Effect of charge ordering and disordering on terahertz radiation characteristics of magnetoresistive  $\text{Pr}_{0.7}\text{Ca}_{0.3}\text{MnO}_3$  thin films. *Opt. Lett.* **29**, 2554–2556 (2004).
10. K. R. Mavani *et al.*, Effects of cation disorder on terahertz emission from half-doped manganite thin films. *EPL* **81**, 17009 (2008).
11. K. Takahashi, N. Kida, M. Tonouchi, Terahertz radiation by an ultrafast spontaneous polarization modulation of multiferroic  $\text{BiFeO}_3$  thin films. *Phys. Rev. Lett.* **96**, 117402 (2006).
12. D. S. Rana *et al.*, Structural dependence of terahertz radiation from multiferroic  $\text{BiFeO}_3$  thin films. *Phys. Rev. B* **77**, 024105 (2008).
13. D. Talbayev, S. Lee, S. W. Cheong, A. J. Taylor, Terahertz wave generation via optical rectification from multiferroic  $\text{BiFeO}_3$ . *Appl. Phys. Lett.* **93**, 212906 (2008).
14. D. J. Hilton *et al.*, Terahertz emission via ultrashort-pulse excitation of magnetic metal films. *Opt. Lett.* **29**, 1805–1807 (2004).
15. E. Beaupaire *et al.*, Coherent terahertz emission from ferromagnetic films excited by femtosecond laser pulses. *Appl. Phys. Lett.* **84**, 3465 (2004).
16. T. Kampfrath *et al.*, Terahertz spin current pulses controlled by magnetic heterostructures. *Nat. Nanotechnol.* **8**, 256–260 (2013).
17. T. Kampfrath *et al.*, Coherent terahertz control of antiferromagnetic spin waves. *Nat. Photonics* **5**, 31–34 (2011).
18. R. V. Mikhaylovskiy *et al.*, Terahertz emission spectroscopy of laser-induced spin dynamics in  $\text{TmFeO}_3$  and  $\text{ErFeO}_3$  orthoferrites. *Phys. Rev. B* **90**, 184405 (2014).
19. R. V. Mikhaylovskiy *et al.*, Terahertz magnetization dynamics induced by femtosecond resonant pumping of  $\text{Dy}^{3+}$  subsystem in the multisublattice antiferromagnet  $\text{DyFeO}_3$ . *Phys. Rev. B* **92**, 094437 (2015).
20. R. V. Mikhaylovskiy *et al.*, Resonant pumping of  $d-d$  crystal field electronic transitions as a mechanism of ultrafast optical control of the exchange interactions in iron oxides. *Phys. Rev. Lett.* **125**, 157201 (2020).
21. M. Tonouchi *et al.*, Ultrashort electromagnetic pulse radiation from YBCO thin films excited by femtosecond optical pulse. *Jpn. J. Appl. Phys.* **35**, 2624 (1996).
22. M. Tonouchi *et al.*, Recent topics in high- $T_c$  superconductive electronics. *Jpn. J. Appl. Phys.* **44**, 7735 (2005).
23. Y. Tominari *et al.*, Resonant terahertz radiation from  $\text{Tl}_2\text{Ba}_2\text{CaCu}_2\text{O}_{8+\delta}$  thin films by ultrafast optical pulse excitation. *Appl. Phys. Lett.* **80**, 3147 (2002).
24. L. Ozyuzer *et al.*, Emission of coherent THz radiation from superconductors. *Science* **318**, 1291–1293 (2007).
25. U. Welp, K. Kadowaki, R. Kleiner, Superconducting emitters of THz radiation. *Nat. Photonics* **7**, 702–710 (2013).
26. E. A. Borodianskiy, V. M. Krasnov, Josephson emission with frequency span 1–11 THz from small  $\text{Bi}_2\text{Sr}_2\text{CaCu}_2\text{O}_{8+\delta}$  mesa structures. *Nat. Commun.* **8**, 1742 (2017).
27. M. Hücker *et al.*, Stripe order in superconducting  $\text{La}_{2-x}\text{Ba}_x\text{CuO}_4$  ( $0.095 \leq x \leq 0.155$ ). *Phys. Rev. B* **83**, 104506 (2011).
28. J. M. Tranquada, B. J. Sternlieb, J. D. Axe, Y. Nakamura, S. Uchida, Evidence for stripe correlations of spins and holes in copper oxide superconductors. *Nature* **375**, 561–563 (1995).
29. E. Berg *et al.*, Dynamical layer decoupling in a stripe-ordered high- $T_c$  superconductor. *Phys. Rev. Lett.* **99**, 127003 (2007).
30. E. Berg, E. Fradkin, S. A. Kivelson, J. M. Tranquada, Striped superconductors: How spin, charge and superconducting orders intertwine in the cuprates. *New J. Phys.* **11**, 115004 (2009).
31. S. Badoux *et al.*, Critical doping for the onset of fermi-surface reconstruction by charge-density-wave order in the cuprate superconductor  $\text{La}_{2-x}\text{Sr}_x\text{CuO}_4$ . *Phys. Rev. X* **6**, 021004 (2016).
32. J.-J. Wen *et al.*, Observation of two types of charge-density-wave orders in superconducting  $\text{La}_{2-x}\text{Sr}_x\text{CuO}_4$ . *Nat. Commun.* **10**, 3269 (2019).
33. J. Lorenzana, G. Seibold, Metallic mean-field stripes, incommensurability, and chemical potential in cuprates. *Phys. Rev. Lett.* **89**, 136401 (2002).
34. H. Miao *et al.*, Formation of incommensurate charge density waves in cuprates. *Phys. Rev. X* **9**, 031042 (2019).
35. D. Nicoletti *et al.*, Optically induced superconductivity in striped  $\text{La}_{2-x}\text{Ba}_x\text{CuO}_4$  by polarization-selective excitation in the near infrared. *Phys. Rev. B* **90**, 100503(R) (2014).
36. E. Casandru *et al.*, Wavelength-dependent optical enhancement of superconducting interlayer coupling in  $\text{La}_{1.885}\text{Ba}_{0.115}\text{CuO}_4$ . *Phys. Rev. B* **91**, 174502 (2015).
37. K. A. Cremin *et al.*, Photoenhanced metastable c-axis electrostatics in stripe-ordered cuprate  $\text{La}_{1.885}\text{Ba}_{0.115}\text{CuO}_4$ . *Proc. Natl. Acad. Sci. U.S.A.* **116**, 19875–19879 (2019).
38. D. Nicoletti *et al.*, Magnetic-field tuning of light-induced superconductivity in striped  $\text{La}_{2-x}\text{Ba}_x\text{CuO}_4$ . *Phys. Rev. Lett.* **121**, 267003 (2018).
39. M. Först *et al.*, Melting of charge stripes in vibrationally driven  $\text{La}_{1.875}\text{Ba}_{0.125}\text{CuO}_4$ : Assessing the respective roles of electronic and lattice order in frustrated superconductors. *Phys. Rev. Lett.* **112**, 157002 (2014).
40. V. Khanna *et al.*, Restoring interlayer Josephson coupling in  $\text{La}_{1.885}\text{Ba}_{0.115}\text{CuO}_4$  by charge transfer melting of stripe order. *Phys. Rev. B* **93**, 224522 (2016).
41. S. Rajasekaran *et al.*, Parametric amplification of a superconducting plasma wave. *Nat. Phys.* **12**, 1012–1016 (2016).
42. L. Dhar, J. A. Rogers, K. A. Nelson, Time-resolved vibrational spectroscopy in the impulsive limit. *Chem. Rev.* **94**, 157–193 (1994).
43. P. E. Dolgirev *et al.*, Theory for anomalous terahertz emission in striped cuprate superconductors. *arXiv:2112.05772* (2021).
44. P. E. Dolgirev *et al.*, Optically-induced Umlapp shift currents in striped cuprates. *arXiv:2203.04687* (2022).
45. H. T. Stinson *et al.*, Infrared nanospectroscopy and imaging of collective superfluid excitations in anisotropic superconductors. *Phys. Rev. B* **90**, 014502 (2014).
46. H. Niwa *et al.*, Light-induced nonequilibrium response of the superconducting cuprate  $\text{La}_{2-x}\text{Sr}_x\text{CuO}_4$ . *Phys. Rev. B* **100**, 104507 (2019).
47. F. J. Dunmore *et al.*, Observation of below-gap plasmon excitations in superconducting  $\text{YBa}_2\text{Cu}_3\text{O}_7$  films. *Phys. Rev. B* **52**, R731–R734 (1995).
48. D. Schumacher, C. Rea, D. Heitmann, K. Scharnberg, Surface plasmons and Sommerfeld-Zenneck waves on corrugated surfaces: Application to high- $T_c$  superconductors. *Surf. Sci.* **408**, 203–211 (1998).
49. A. Tsiatmas *et al.*, Superconducting plasmonics and extraordinary transmission. *Appl. Phys. Lett.* **97**, 111106 (2010).
50. A. Tsiatmas, V. A. Fedotov, F. J. G. de Abajo, N. I. Zheludev, Low-loss terahertz superconducting plasmonics. *New J. Phys.* **14**, 115006 (2012).